Supporting Information

Fabrication of Microfluidic Chips Using Laser Click Deposition

Mengqi Lv, Xinyu He, Kai Zhou, Ben Niu, Wei Wei, Haoran Li, Shasha Liu, Hua Su, and Wei Wang*

State Key Laboratory of Analytical Chemistry for Life Science, Chemistry and Biomedicine Innovation Center (ChemBIC), School of Chemistry and Chemical Engineering, Nanjing University, Nanjing 210023, China

*Corresponding authors

Table of Contents

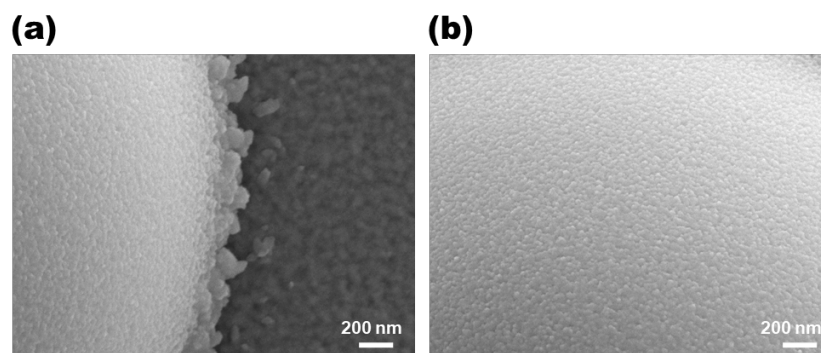**S1. Characterization of the deposition materials**

(a) **(b)**

Figure S1. Partially magnified SEM image of the deposition material obtained from LCD (50000× magnification). (a) Surface and (b) Edge of the deposited CuO. The scale bar is 200 nm.

S2. The influence of the precursor solution on the composition of the deposited materials
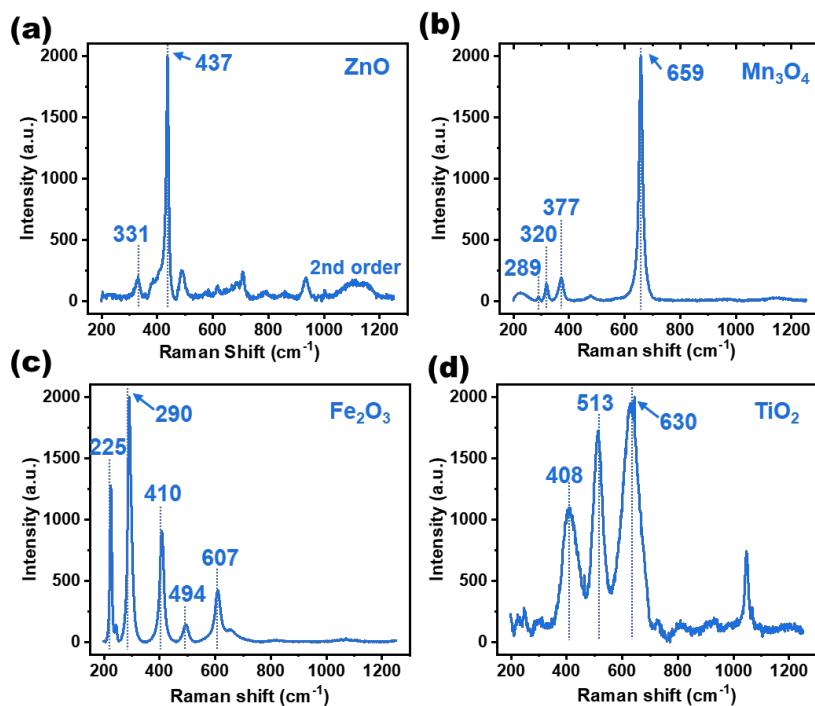

Figure S2. Raman spectra of transition metal oxide materials obtained by the laser click deposition technique. (a) Deposited ZnO with 50 mmol/L Zn(Ac)$_2$ as the precursor solution. (b) Deposited Mn$_3$O$_4$ with 50 mmol/L Mn(Ac)$_2$ as the precursor solution. (c) Deposited Fe$_2$O$_3$ with 20 mmol/L Fe(Ac)$_2$ as the precursor solution. (d) Deposited TiO$_2$ with titanium oxysulfate-sulfuric acid hydrate as the precursor solution.

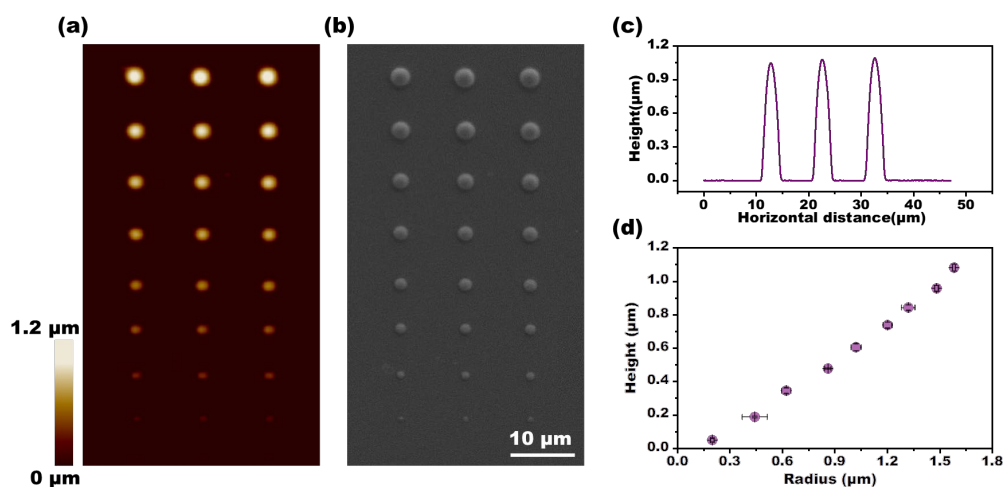## S3. The dependence of the deposition thickness on laser parameters

Figure S3. (a) AFM image and (b) SEM image of the CuO particle array at various laser powers. The growth conditions change vertically, while the growth conditions in each row are identical. From top to bottom, the laser power is 8.6 mW, 8.1 mW, 7.6 mW, 7.0 mW, 6.5 mW, 6.0 mW, 5.4 mW, 4.9 mW, and 4.3 mW, with the present deposition time set at 2 s. The scale bar is 10 μm. (c) The first row cross-section changes in height. The standard deviation of the three deposited particles' height in the first horizontal column is 0.02 μm. (d) The scatter plot reveals the relationship between height and radius, with both vertical and horizontal error bars at each data point. The error bars represent the standard error range. Deposition height appears to have a clear positive correlation with the radius.
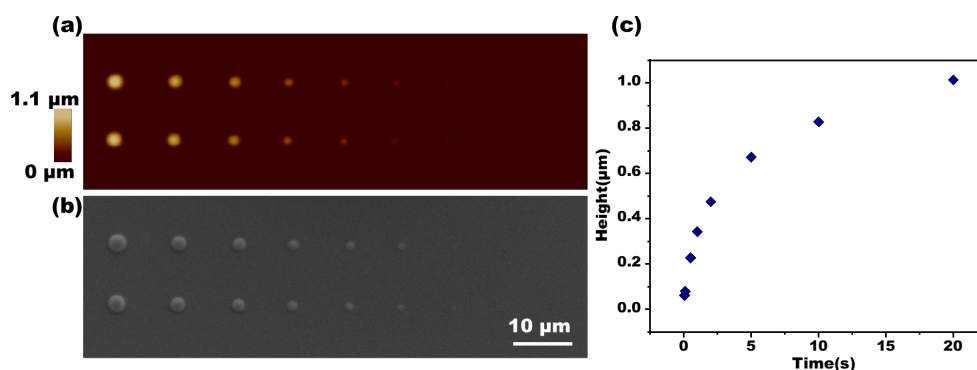

Figure S4. (a) AFM image and (b) SEM image of the CuO particle array under various exposure times. The growth conditions change horizontally, while the growth conditions in each column are identical. From left to right, the exposure time is 20 s, 10 s, 5 s, 2 s, 1 s, 0.5 s, 0.1 s, 0.05 s, with the present laser power set at 6.0 mW. The scale bar is 10 μm. (c) The evolution of the instantaneous height of the CuO microstructure with time. The deposition heights appear to have a clear power law relationship with the exposure time.

S4. The feasibility of constructing the laser click deposition process on various substrates
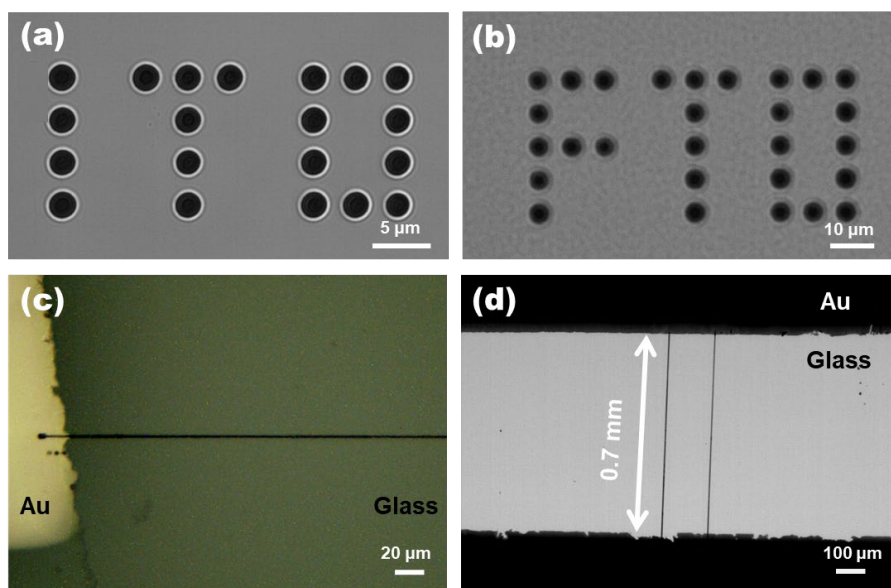

Figure S5. (a) Bright field image of CuO particles deposited on the ITO substrate. The scale bar is 5 μm. (b) Bright field image of CuO particles deposited the FTO substrate. The scale bar is 10 μm. (c) Color bright field image and (d) monochromatic bright field image of a micron-sized CuO bridge deposited on the gold/glass interface, The scale bars are 20 μm and 100 μm, respectively.
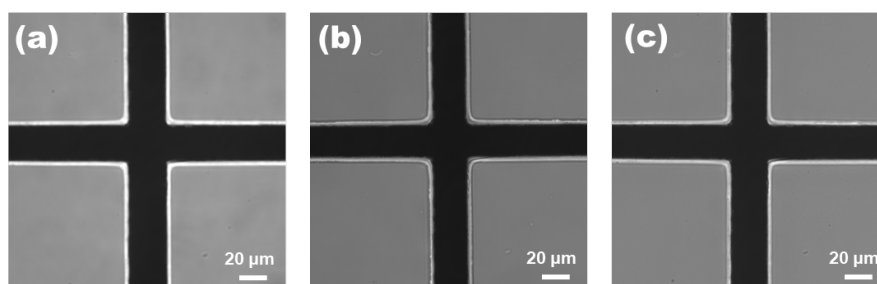
Figure S6. A bright field image of the master mold under the continuous process of casting, curing, and peeling. (a) The initial master mold, (b) The master mold after one casting and curing cycle. (c) The master mold after 10 cycles. The master mold is carefully examined before being used, and there is no skin shedding or deformation. The casting processes allow the production of crack-free structures in the master mold while preserving good dimensional accuracy and surface flatness.
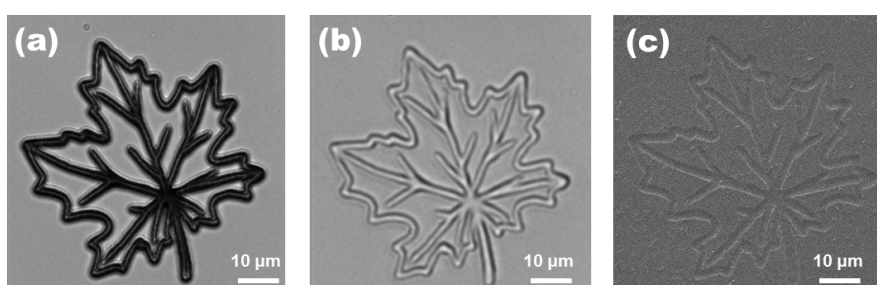

Figure S7. (a) Bright field image of a designated copper oxide pattern. (b) Bright field image and (c) SEM image of the corresponding leaf-like microchannel. The scale bar is 10 μm. There is no pattern deformation occurring, especially when removing the cast from the mold.

S6. Description of Movies

Movie S1. Movie of the whole deposition process detected by bright field microscopy in Figure 4a

Movie S2. Bright field imaging of the micro-QR code fabrication process in Figure 5a